ECS Journal of Solid State Science and Technology, 2023 **12** 043012
2162-8777/2023/12(4)/043012/9/$40.00 © 2023 The Electrochemical Society ("ECS"). Published on behalf of ECS by IOP Publishing Limited

Structural, Thermoelectric, Electronic, and Magnetic Properties of Pristine Intermetallic Rare-Earth-Based XMn_2Si_2 (X=Dy, Er) Compounds

Zeshan Zada,[1] Junaid Khan,[2] Abdul Ahad Khan,[3] Ali H. Reshak,[4,5,6,z] Dania Ali,[7] Fazal Ur Rehman,[8] Inayat Urrahman,[1] Muhammad Saqib,[9] Muhammad Irfan,[10] and Muhammad M. Ramli[5]

[1]*Materials Modeling Lab, Department of Physics, Islamia College University, Peshawar 25120, Pakistan*
[2]*Department of Physics, Khushal Khan Khattak University, Karak, Pakistan*
[3]*Department of Physics, University of Peshawar, Peshawar 25120, Pakistan*
[4]*Physics Department, College of Science, University of Basrah, Basrah 61004, Iraq*
[5]*Center of Excellence Geopolymer and Green Technology (CEGeoGTech), University Malaysia Perlis, 01007 Kangar, Perlis, Malaysia*
[6]*Department of Instrumentation and Control Engineering, Faculty of Mechanical Engineering, CTU in Prague, 616607 Prague, Czech Republic*
[7]*Faculty of medicine, Charles University, Pilsen 30100, Czech Republic*
[8]*Department of Chemistry, Lahore Garrison University, Lahore, Pakistan*
[9]*Department of Electrical and Computer Engineering, COMSATS University Islamabad, Abbottabad Campus, Abbottabad 22060, Pakistan*
[10]*Department of Physics, University of Sargodha, Sargodha, Punjab, Pakistan*

Detailed Structural, thermoelectric, electronic and magnetic properties of the ternary rare-Earth based XMn_2Si_2 (X=Dy, Er) Compounds, are investigated using the full-potential linearized augmented-plane wave (FP-LAPW) method with generalized gradient approximation (GGA+U) in ferromagnetic phase. The basic calculations of optimization are found with the support of (PBE-GGA) to realize theoretical consistency with existing experimental consequences, although for the enhancement of magneto-electronic part the (GGA+U) technique is employed. We have identified theoretically that the ferromagnetic is the most suitable phase among three studied phases for these compounds agree well with previous experimental works. The electronic band structure indicates that these compounds are metallic through both spin channels in the FM phase. A secure hybridization occurs between the elements Dy/Er-f and Mn-d states in the valence band and the Si-p state in the conduction band. The total magnetic moments verify that the rare-Earth based $DyMn_2Si_2$ ternary inter-metallic compound showcases stronger ferromagnetic behavior patterns than the $ErMn_2Si_2$ compound. We estimated the Seebeck coefficient S, electrical and thermal conductivities, and the ZT in this study over the temperature range of 0 to 800 K. The $ErMn_2Si_2$ is a viable contender for high-temperature applications in waste heat management because of its high ZT values in the high-temperature region in thermoelectric devices.
 [DOI: 10.1149/2162-8777/acccaa]

Manuscript submitted January 31, 2023; revised manuscript received March 1, 2023. Published April 24, 2023.

The pristine intermetallic materials (zintl) have their precise electronic structure that continues to construct them responsible for numerous advanced attributes at the quantum level side.[1–5] Nowadays, the interest in the direction of the exploration of materials containing intermetallic phases have become more common due to their intriguing characteristics and different wide range applications and featuring new approaches like shape memory alloys, in jewelry and dentistry[2,3] innovative computer read along with their inspirational utilization by way of "colossal-magneto resistive (C-M-R)" or "giant-magneto-resistive consequence".[6,7]

Usually, the magnetoresistance is metallic thin films, which are able to vary the resistivity in relation to the external field.[8–14] The G-MR are diverse applications like spin values, spin filter, are also a key role in the major magnetic field sensor.[15,16] Many symmetries of intermetallic phases (Zintl) are found and are more important for the material magnetic properties, which are a highly valuable phase for the single-molecule magnetics and read head.[7,17]

The Intermetallic phases having formula of BL_2X_2 (where B (rare/alkaline-Earth metals), L (d-block metals); whereas X be a member of Group 13–15 elements) lies in two persistent types of structure, having space groups specifically $ThCr_2Si_2$ (14/mmm) and also $CaAl_2Si_2$ (P3m1) correspondingly. However, these are employed in previous research to examine different physical aspects of intermetallic (zintl phase) compounds.[7–10,12,14,16]

Recent years have seen a lot of research interest in the ternary intermetallic compounds with the stoichiometric ratio of 1:2:2 and a formula with representation RT_2X_2 where (R)-rare Earths, (T)-transition metals and (X)-p block elements, respectively.[18] Due to the presence of wide range of intriguing physical features, including superconductivity, effect of heavy fermion, intermediate valence, magnetic complex structures along with several transitions, and so on.[19,20] Furthermore, the magnetic-ordering that develops from the (3d) manganese (Mn) subsystem at higher temperature ranges[21] makes the compounds generated when T=Mn particularly fascinating in terms of their magnetic characteristics. Investigations into the RT_2X_2 family for magnetocaloric effect (MCE) have recently been carried out in various works. As a result, various compounds, including $TbMn_2Si_2$[22] and ErT_2Si_2 (T=Mn, Cu and Cr),[23] have been found to have enormous MCE.

The compounds $DyMn_2Si_2$ and $ErMn_2Si_2$ belongs to RT_2X_2 family with attracting magnetic features. The first material was synthetized by D. Rossi et al. in 1978,[24] while the later one was synthetized and characterized in 1981 by Szytuła, A. and I. Szott.[25] as a tetragonal (body centered) structure. Generally, the compounds are totally based on a bonding nature like Mn_2Si_2 is covalent with a large charge transfer of R^{2+}. The structure is stable due to one-layer charge being $[Mn_2Si_2]^{2-}$ and others are parted by (non-magnetic) R^{2+} cations, which show the magnetic effect. Later, an antiferromagnetic ordering and an extra magnetic phase around 473 and 55 K were discovered in the $DyMn_2Si_2$ combination by means of magnetic analysis.[25] A complicated structure with numerous magnetic possible transitions at temperature underneath 85 K linked to long range dysprosium interaction and canted manganese (Mn) moment was shown by magnetic and Mossbauer experiments.[26] Additionally, an AFM transition related to Mn-Mn interaction was seen at 511 K. Moreover, four transitions for $DyMn_2Si_2$ at low temperatures ($T < 100$ K) are reported by Ono and co-authors.[27] The

[z]E-mail: maalidph@yahoo.co.uk

magnetization curve's, though, differs significantly from the findings presented in the reference[26] at low magnetic (B) fields and reported weak ferromagnetic transitional (83.4 K) temperatures. According to the authors, the found discrepancy is caused by a significant magnetic anisotropy. Subsequent magnetic experiments on $DyMn_2Si_2$ single crystals[28] revealed a magnetic-transition at 44 K (a temperature lower than the only transition detected by Szytuła, A. and I. Szott[25]) and three lower-temperature differences.

The X-ray diffraction and magnetization findings have been used to explore the magnetic, structural, and magnetocaloric features of the intermetallic ternary $DyMn_2Si_2$ material. Furthermore, the proximity of two subsequent transitions, caused a table-like magnetocaloric effect (MCE) throughout a large temperature range.[29] As a result, the unusual magnetic characteristics of the compound $DyMn_2Si_2$ were intriguing for low temperature range magnetic refrigeration.

Due to their exceptional physical features and possible uses as high temperature thermo-electrics, $REMn_2Si_2$ (RE = Rare Earth) crystals have piqued the curiosity of many researchers.[30] Solid-state reaction and techniques of arc-melting were used to create ternary RE-manganese silicides.[31] Lead-based metal flux synthesis offers the quickest way to create single crystals of ternary RE-transition metal silicides. In earlier research, the researcher described the lead flux synthesis conditions for YMn_2Si_2, and[32] $ErMn_2Si_2$ crystals.

Later, Okada, Shigeru, et al. described the experimental setup for producing comparatively large single crystals of $REMn_2Si_2$ from a high-temperature lead flux in an argon environment.[33] The middle section of the lanthanide series was chosen. The compounds belong to these families can crystalize in a variety of structure types, which favors the existence of diverse magnetic and electrical properties. Depending on the T and X elements, the researchers have found that the temperatures range from low <2 K to high >300 K for observing magnetic ordering in these compounds.[34] Additionally, significant magnetocaloric impact and magnetoresistance were found in numerous compounds belonging to these families. These mentioned properties make these compounds suitable candidates for use in magnetic refrigeration.

The $DyMn_2Si_2$ compound showed complex magnetic structure along with multi-magnetic transitions. Mn ions in the compound exhibit antiferromagnetic (AFM) order at high temperature TN $\sim$ 425 K. Three magnetic-phase transitions were achieved for the compound $DyMn_2Si_2$ at temperatures below $T < 40$ K.[35] The apparent transition around 38 K is attributed to a long-range (ferromagnetic) interaction among (Dy-Dy) ions, based on the neutron diffraction and Mossbauer results, while $T_1 \sim 31$ K can also be connected to a canted (ferrimagnetic) transition resulting from such a long-range exchange mechanism among magnetic (Dy-Dy) and (Mn-Mn) sub-lattices.[36,37] The antiferromagnetic anomaly identified around $T_2 \sim 20$ K is linked to modifications with in AFM structure of the Mn sub-lattice.

The $ErMn_2Si_2$ and $ErMn_2Ge_2$ compounds displayed ferromagnetic/anti-ferromagnetic characteristics at low/high temperatures, according to magneto metric experiments on polycrystalline samples.[38] The $ErFe_2Ge_2$ compound stays paramagnetic at 4.2 K,[39] While $ErFe_2Si_2$ compound ordered antiferromagnetically just at Neel temperature of 2.6 K.[40] A rise in the intensity of over-all reflections is evident here in the neutron diffraction pattern recorded at low temperature 4.2 K, suggesting that a ferromagnetic ordering exists. It was established by the examination of the intensities that the magnetic moments ($\mu_{Er} \approx 9\ \mu B$) are confined to Er atoms and are aligned to the c-axis perpendicularly.[41] In the range of temperature from 1.8 to 293 K, a neutron diffraction analysis of the polycrystalline compounds was conducted.[41] An array $+ - + -$ of ferromagnetic layers composed of Mn atoms make up the antiferromagnetic collinear structures of $ErMn_2Si_2$ and $ErMn_2Ge_2$ both at RT and LNT. The magnetic moment with value ($\approx 2\ \mu B$) of Mn atom in these compounds are parallel to the c-axis.

So far, various properties have been observed to be dependent primarily on constituent element or composition.[42] Interestingly, a significant MCE was found in the RT_2X_2 series compounds.[43,44] This MCE was linked to a field-induced first order magnetic transition from an antiferromagnetic to a ferromagnetic state. Studies of magnetism and heat capacity have been utilized to analyze the magnetic characteristics and magnetocaloric effect (MCE) in the ternary $ErMn_2Si_2$ compound. The calculated magnetization with value at 2 and 7 T was 7.92 μB, which was significantly less than the saturated magnetic moment (9.0 μB) of a free Er^{+3} ion.[20] The value of the (Mn) moments and the magnetic phase of the Mn sublattice are highly sensitive to the interatomic (Mn-Mn) distance, $d_{Mn\text{-}Mn}$, for said RMn_2X_2 (X = Si/Ge) systems.[44] The magnetic alignment along the c-axis in neighboring Mn is ferromagnetic whenever $d_{Mn\text{-}Mn}$ is bigger than critical values of $d_{Mn\text{-}Mn}$ ($\sim$2.85 Å), while antiferromagnetic at low values, based on the interlayer coupling (ITC) model.[45]

The magnetic ordering transition, which was also validated by the magnetization measurement, is what causes the k-shape spike too appeared about 4.5 K in specific heat C(T) curves beneath zero field. At the same temperature 4.5 K, a second order magnetic phase transition from paramagnetic to ferromagnetic has additionally been detected along with a large reversible MCE.[20] Furthermore, the heat capacity C of $ErMn_2Si_2$ at fields of 0, 1, and 5 T was observed to be low temperature dependent magnetic refrigeration. According to the data that has been so far reported, both the reported discrepancy in the magnetic behavior in addition to the complicated magnetic parameters remain to be explained properly of these compounds.

There is no theoretical work in the literature from the above discussion present on pristine rare Earth based XMn_2Si_2 compounds. However, some experimental work has already been reported on rare-Earth based compounds because of their interesting physical properties such as superconductivity, magnetic order, heavy-fermion capabilities, valence fluctuations, giant MCE, and so on.[19,20,42] Currently, we focused first on the structure, thermoelectric, electronic and magnetic properties. This was partially inspired by a research gap of XMn_2Si_2 (X=Dy, Er) compounds by employing the FP-APW method. We have calculated all these parameters by using the DFT and linked them with the existing results in the literature.

Computational Detail

Computationally these calculations were achieved for XMn_2Si_2 by using density functional theory (DFT).[46–50] The calculation was carried out for the full potential linearized augmented plane wave (FPL-APW) as defined by the Wien2k code.[51] In order to analyze exchange and correlation potentials, generalized gradient approximations (GGA-PBE)[52] and GGA+U[53,54] are used. The improved results, especially for electronic and magnetic features, are then compared among the noted approximations for best possibilities. The application of the spin-polarized (GGA+U) technique,[53] which also incorporates an on-site Coulomb repulsion, is the only possible way to further increase the clarity of presentation of d/f localized electrons. We have used $U_{eff} = 7$ eV[9,12] for the XMn_2Si_2 compounds in order to treat only the d and f states. Moreover, spherical harmonics were organized together with aid of two steps to implement, i.e., (E-D) electronic-densities and probably potential. The charge density was Fourier expanded up to the $G_{max} = 12$ atom unit $(au)^{-1}$ for these two potentials by circular atomic sites with a cutoff value of $l_{max} = 10$. Where G_{max} shows the leading vector in Fourier expansions. By using the scalar-relativistic approach, wave functions are increased to extend in the interstitial domain (ID) to plane waves with a cutoff value of $R_{MT} \times K_{max}$ was set to 7.0. The R_{MT} provided the average radius of muffin-tin spheres while K_{max} provided larger magnitude K vector values inside the plane wave. We chose the value of non-overlapping muffin-tin radii for these element as (2.4, 2.0, 1.9) and (2.4, 2.0, 1.9) for (Dy, Mn, Si) and (Er, Mn, Si) in "au" in that order respectively. We proposed the 1000 k points[55–57] Monkhorst–Pack mesh in the irreducible Brillouin Zone for rare-Earth based XMn_2Si_2 compounds. Moreover, its thermoelectric properties have now been studied using the semi-classical

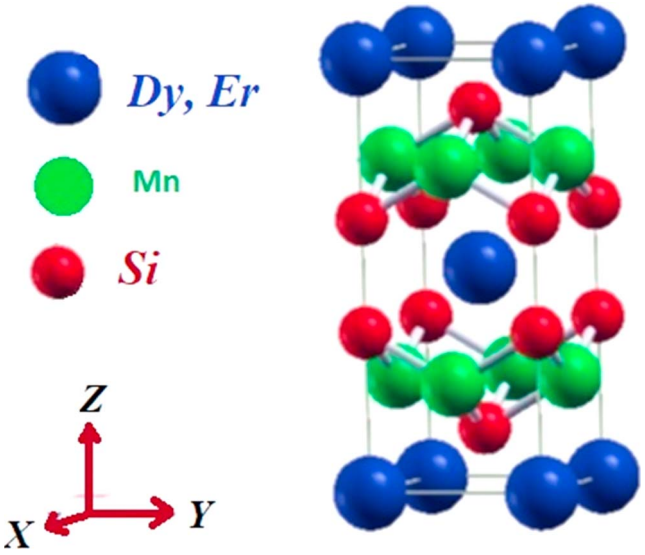

Figure 1. Crystal Structure of XMn_2Si_2 (X=Dy, Er) Compounds.

Boltzmann transport theory, which is performed in the Boltztrap program.[58–60]

Result and Discussion

Structure properties.—In this section, the structure properties of XMn_2Si_2 (X=Dy, Er) clarify distinct structure parameters like lattices constant, bulk modulus, binding energy or optimization energy, and unit cell volume.

According to the studies, the XMn_2Si_2 crystallizes in a tetragonal $ThCr_2Si_2$-type structure with a (I4/mmm) space group, in which the atoms of an elements Dy/Er, Mn, and Si, respectively, occupying the (2a), (4d), and (4e) positions. In these structures, the atoms are organized to create a series of X-Mn-Si-Mn-X-Mn-Si-Mn-X planes that are perpendicular to the tetragonal c-axis and contain the same kind of atoms. The Dy/Er atoms located in the core of the tetragonal unit cell are surrounded by eight (Mn and Si) each atom from adjacent layers. The optimization process is formed by relaxed geometry in Fig. 1. The optimization process is performed in three different phases i.e. Paramagnetic (P-M) Phase, the ferromagnetic (F-M) Phase, antiferromagnetic (AF-M) Phase. The structure parameters are investigated by means of geometry volume-optimization process for the reported materials. The total energy of XMn_2Si_2 (X=Dy, Er) is investigated among three phases under (GGA-PBE) approximation. There is no descriptive experimental and theoretical study on XMn_2Si_2 (X=Dy, Er). Therefore, the structural stability is calculated from ground state energy. The ground state energy is calculated using the following expression

$$E_f = E_{tot} - E_X - 2E_{Mn} - 2E_{Si} \quad [1.1]$$

The E_{tot} is the total ground energy of XMn_2Si_2 (X=Dy, Er), while $E_X - 2E_{Mn} - 2E_{Si}$ are the total energies for each X= (Dy, Er), Mn, and Si, respectively. The negative value of the ground state energy in Table I indicates that XMn_2Si_2 (X=Dy, Er) are thermodynamically stable. The achieved lowest ground state energy of these compounds is in ferromagnetic phase in comparison with other calculated Paramagnetic and Antiferromagnetic (PM/AFM) phases. Due to the optimized plot as shown in Fig. 2 and calculation of energy, the structure as shown in Fig. 1 stabilizes in the ferromagnetic phase. Moreover, the calculated results show that XMn_2Si_2 (X=Dy, Er) are favorable materials for the ferromagnetic configuration. The compounds' structural characteristic behavior is governed by determining atomic lattice locations as well as cell dimensions. Our calculated structural data (Table II) theoretically agree well with previous experimental works[20,24,33,61] that have reported the ferromagnetic response of the materials, particularly at low temperatures.

We currently have only experimental lattice constants as cited above for both compounds to compare, as well as volume for $DyMn_2Si_2$, to support our findings. In the structure when the Er Cation is substituted by Dy atom, the values of (a and c (Å)), (V_0) and B decrease as the three different (PM, FM and AFM) phases are calculated. This noted reduction is due to decrease in the atomic sizes of the cations as one move in the period from Dy to Er element. Lastly, the bulk modulus (B), which measures compressibility, exhibits a clear downward trend from Dy → Er, making $ErMn_2Si_2$ a more compressible combination than $DyMn_2Si_2$.

Electronic properties.—The band structure and density of states of XMn_2Si_2 (X=Dy, Er) compounds with up and down spin channels is determined by (PBE-GGA) in Figs. 3a, 4a and (GGA +U) potentials in Figs. 3b, 4b respectively. The band structure of these compounds is interviewed by symmetry points (Γ, H, N, Γ, P) of the Brillouin zone, while the calculated TDOS and PDOS are plotted in the range of energy between −6 eV and 6 eV, to conceptualize the electronic features of the physical structure.

The significant dispersion of three valence bands maximum at the symmetry high H point is clearly observed. By applying PBE-GGA potential, all three bands dominantly emerge while passing the Fermi level, hitting or touching the conduction band, and remaining in the region in spin up channels of XMn_2Si_2. While the few valence bands maximum displays dispersion along both basal-plane Γ−H and Γ−N directions spin down channel of XMn_2Si_2, and most surprisingly, also on the c-axis, the Γ−P line. This indicates that almost all directions are likely to have excellent conductivity for XMn_2Si_2. Additionally, for both of the studied compounds, a band with a gap appears at Γ, below as near the valence band maxima. The presence of such multiband behavior is indeed a dominant beneficial feature of thermoelectric materials.

Furthermore, the disappearance of two valence bands through (GGA+U) with a single band appearance and shoulder on both side at high (H point) symmetry in XMn_2Si_2 compounds. Additionally, single band dispersion has become more prominent of conduction band minimum at (N and Γ−P basal points) spin up channel. While both the compounds follow the (PBE-GGA) potential in spin down channel where few maxima of valence bands and minima of conduction bands show dominant dispersion along basal-plane Γ −H, Γ−N and Γ−P directions.

In spite of this, the conduction band minimum of XMn_2Si_2 follows the similar trend, with a dominant single band dispersion at high (N) symmetry point via the (GGA+U) from up-spin channel while stay within the region through (PBE-GGA) of conduction band (which denotes that the conduction bands are fully filled and do not contain any further electrons) with the absence of an overlapping-mechanism is observed with the valence bands.

The bands clearly split whenever the GGA+U is computed, although both rare-Earth-based XMn_2Si_2 compounds continue to show their metallic character. The valence band drops down and the conduction band goes up at the high symmetry (Γ point) by bounding d-states while computing the GGA+U approximation.

Additionally, there exists no energy gap (absent gap) at the Femi level, expressing the nature of being purely metallic, whereas bands in spin-up channels are significantly closer to one other than spin-down channels nearby the Fermi energy level. Although these adjacent states allow for easy electron mobility, this also has a long-term effect on the system's conductivity. Due to the crossing band mechanisms overall the Fermi level as well as the absence of a gap for both channels of spin when analyzing (PBE-GGA and GGA +U) separately, the rare-Earth based XMn_2Si_2 (X=Dy, Er) compound band structures overall tend to represent full-metallic nature.

Due to the observed total and (p, d, and f) partial states that crossed the Fermi level of energy in both channels of spin dominatingly, both the understudy compounds exhibit full metallic

Table I. Calculated lattice parameters, *a* (Å), *c* (Å), ground-state volume *V0* (a.u)^3, Bulk modulus *B* (GPa) for ferromagnetic XMn_2Si_2 (X=Dy, Er) ternary compounds.

Compounds	Lattice constant $(A)^0$		$V_0(a.u)^3$	B(GPa)	Bp	E_o		
	a	C				FM	AFM	PM
$DyMn_2Si_2$	3.924	10.421	532.1491	128.5707	5	−30131.7587	−30131.6513	−30131.5
Exp[a,b,c)]	3.918[a)]	10.438[a)]	160.23[a)]					
	3.915[b)]	10.440[b)]	160.0[b)]					
	3.923[c)]	10.453[c)]	160.9[c)]					
$ErMn_2Si_2$	3.882	10.415	528.9282	125.5115	5	−31994.4761	−31994.43	−31994.37
Exp[d)]	3.896[d)]	10.415[d)]						

a) Ref.[33] b) Ref.[24] c) Ref.[62] d) Ref.[20]

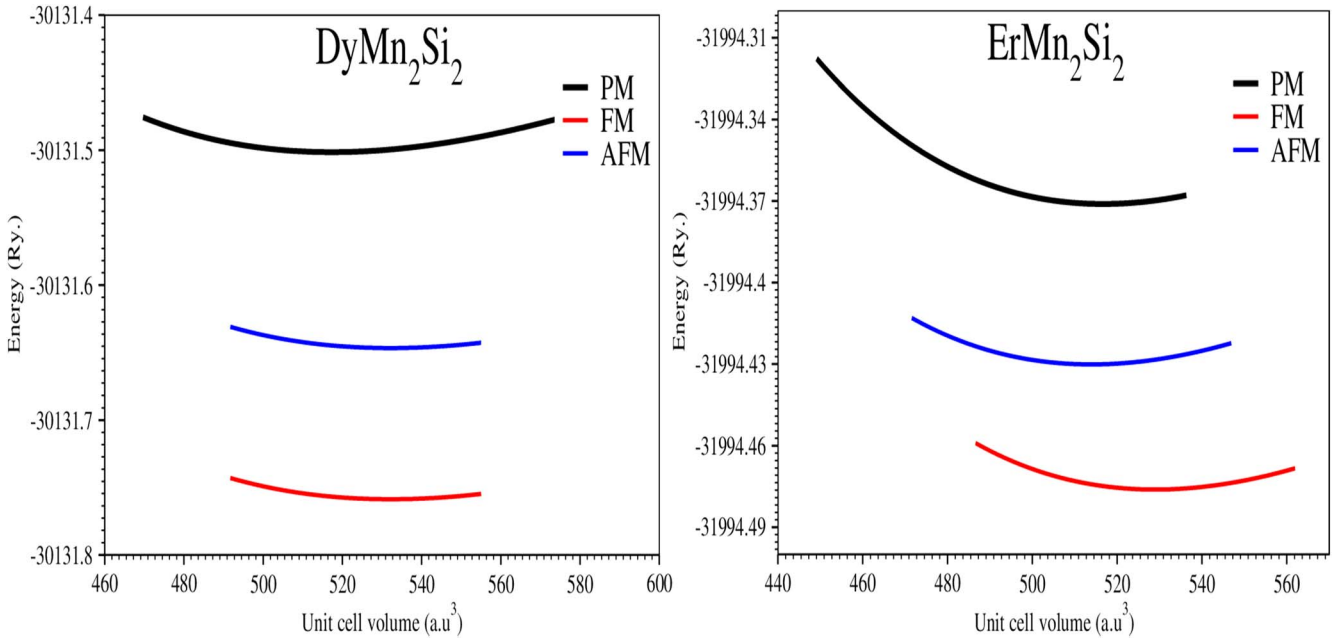

Figure 2. Optimization plots showing energy verses unit cell volume XMn_2Si_2 (X = Dy, Er) Compounds.

behavior. As a result, we may infer from Figs. 4a, 4b that the orbital contribution in Ferro-magnetic phase XMn_2Si_2 (X = Dy, Er) is really quite comparable.

Additionally, it is easy to see from the DOS in which the current activity is at (EF) frequently originates from Mn-d state. Moreover, the elements Dy/Er-f and Mn-d states in the valence band and the Si-p state in the conduction band exhibit substantial hybridization. Such conditions are the cause of the metallic characteristics of the materials.

Both the Dy/Er-f and Mn-d states have prominent occurrence and participation at the Fermi energy level, as well as XMn_2Si_2 compounds dominant spread from high to low energy in the area of valence band. The usage of the (GGA+U), which handles localized f/d-shell electrons of the Dy, Er and Mn atoms, is what causes the f/d-states for both compounds to shift toward lower energies in the up-spin channel while staying in the same positions in the down spin channel.

Furthermore, the disappearance of the Dy/Er-f and Mn-d states from spin up channels at even further lower in energy by utilizing (GGA-PBE) and higher in energy by utilizing (GGA+U) in the valence band region and further higher in energy in the conduction band region by using both potentials, while the appearance of the same Dy/Er-f and Mn-d states at or near the fermi level through down spin on both sides by computing (GGA-PBE) and (GGA+U) is evidently shown in compound DOS plots. Similarly, Si-p state in the region of the valence and conduction bands across the noted energy range via both potentials makes a negligible contribution. According to previously published research,[2] the employed value for XMn_2Si_2 is (U=6 eV), which is a highly accurate estimate to cope with the f and d states of the Dy/Er and Mn atoms, respectively.

In contrast, there is no any sharp appearance, but there is a slight contribution to the various spin states of XMn_2Si_2 from the X-f and Mn-d states in the vicinity of the conduction band, as shown using the GGA-PBE and GGA+U potentials. Curiously, the XMn_2Si_2 compounds essentially non-symmetric appearance in their multiple states (X-f, Mn-d, and Si-p) spectra by both channels, which reside in valence and conduction bands, contradicts the stoner argument's.[4,7,12,16]

Magnetic properties.—Spin polarized computations using the PBE-GGA and GGA+U potentials are used to examine the magnetic properties of XMn_2Si_2 (X=Dy, Er) compounds. The Table II provides an overview of the individual (Dy/Er, Mn, and Si) and interstitial magnetic moments, (total for each cell m^c) magnetic moments of the rare-Earth based compounds under consideration.

According to the tabulated data, Dy/Er and Mn atoms are the greatest effective contributors to the total cell of XMn_2Si_2 magnetic moment, having strong parallel ferromagnetic values, as opposed to Si atoms, which are making an antiparallel influence through both potentials. Therefore, all additional sites besides the silicon (Si) site contribute to enhancing the overall ferromagnetic character of the aforementioned compounds.

Table II. Calculated total, interstitial and local magnetic moments of $DyMn_2Si_2$ and $ErMn_2Si_2$ compounds with both (PBE-GGA and GGA+U) potentials.

Compound	$m^{interstial}$	$m^{Dy/Er}$	m^{Mn}	m^{Si}	m^{cell}
$DyMn_2Si_2$ (PBE-GGA)	0.15375	4.75813	1.69901	−0.05546	8.19898
(GGA+U) Exp	0.25300	4.73943	3.69418	−0.11059	12.15961
$ErMn_2Si_2$ (PBE-GGA)	0.12747	2.50885	2.04071	−0.07047	6.59558
(GGA+U)	0.30667	2.50885	4.04746	−0.11904	10.67237
Exp[a)]	–	–	–	–	9.0[a)]

[a] Ref. 20.

Additionally, the ferromagnetic nature of the stable magnetic ground state is supported by the (non-negative) values of the net-magnetic moments of the $DyMn_2Si_2$ and $ErMn_2Si_2$ compounds by utilizing both the PBE-GGA and GGA+U potentials, as shown in the optimization graphs in Fig. 2 and previously published research investigation[2,4,16] for the both rare-Earth based compounds. Due to the ferromagnetic character, both in our calculation and in earlier research,[20,24,33,61] the parallel magnetic moment for these compounds is the main focus of our work.

Besides this, the computation based on the GGA+U produces a value with such a larger magnitude in contrast to certain other approximation potentials that have been previously identified since it primarily agreements with localized (f and d-shell) electrons of the Dy/Er and Mn atoms and rises their magnetic moment to a lesser extent than the PBE-GGA.

In addition, the interstitial site and individual (Dy/Er, Mn, and Si) atoms encourage the overall net moment, whereas the Si site opposes it, based on the measured values of XMn_2Si_2 compounds magnetic moment by both potentials, as shown in Figs. 4a, 4b. This is because Dy/Er-f and Mn-d states emerge most frequently over the noted energy range. The antiferromagnetic interaction in between valence-band electrons is seen by the opposing sign appearing in the magnetic moments of the Inst, Dy/Er, Mn, whole cell, and Si elements.

Because Dy and Mn are perfectly aligned with the compounds net magnetic moment, $DyMn_2Si_2$ exhibits higher ferromagnetism. As seen in Table II, the value of m^{Mn} changes from (1.69901) to (3.69418) when the d states of the Mn atom are bound by the GGA +U potential.

At last, because of the differences in electro negativity between the atoms of Dy (1.22) and Er (1.24), the total magnetic-moments align parallel through both approximation potentials verify that the rare-Earth based $DyMn_2Si_2$ ternary inter-metallic compound showcases stronger (ferromagnetic) behavior patterns than the $ErMn_2Si_2$ compound. As a result, the greater overall electronegativity difference, the higher the magnetic-moment in magnitude demonstrated by the $DyMn_2Si_2$ compound, indicating stronger ferromagnetism.

Thermoelectric Properties.—BoltzTraP is the algorithm used to compute thermoelectric parameters based on semi-classical Boltzmann theory.[58–60] For thermoelectric materials, particularly those used in detectors and cooling equipment, low and high temperature refrigeration, thermal energy provides a source for the creation of electrical energy. A material is said to be more efficient if it contributes less thermal conductivity and higher electrical conductivity and Seebeck coefficient. We estimated the Seebeck coefficient S, electrical and thermal conductivities, and the ZT in this study over the temperature range of 0 to 800 K.

In a thermoelectric device, electrons can go from an area of high temperature to one of low temperature because high temperature produces greater thermal energy. According to the band structure and density of states shown in Figs. 3a, 3b and 4a, 4b, electrical conductivity is the movement of free charge carriers. Figure 5 shows that excited electrons in XMn_2Si_2 contribute to electrical conductivity. The $DyMn_2Si_2$ and $ErMn_2Si_2$ exhibit a clear reduction in electrical conductivity because the collisions between electrons and positive metal ions become more rapid, lowering the relaxation time and resistivity as a result within a specific temperature range. It is the second-most significant factor in heat conversion, following temperature, and it depends on free electrons and lattice vibrations to create thermal conductivity. Free charge carriers are primarily responsible for the production of heat transmission in the case of semi-conductors and metals.

The compound $DyMn_2Si_2$ exhibits a progressive rise, whereas $ErMn_2Si_2$ exhibits a steady decrease from their initial starting values until 150 K, after which a gradual decrease is observed throughout the temperature range covered by the study. Interestingly, both compounds share the same magnitude at 600 K before reaching their minimum at 800 K. Additionally, at the initial and final given

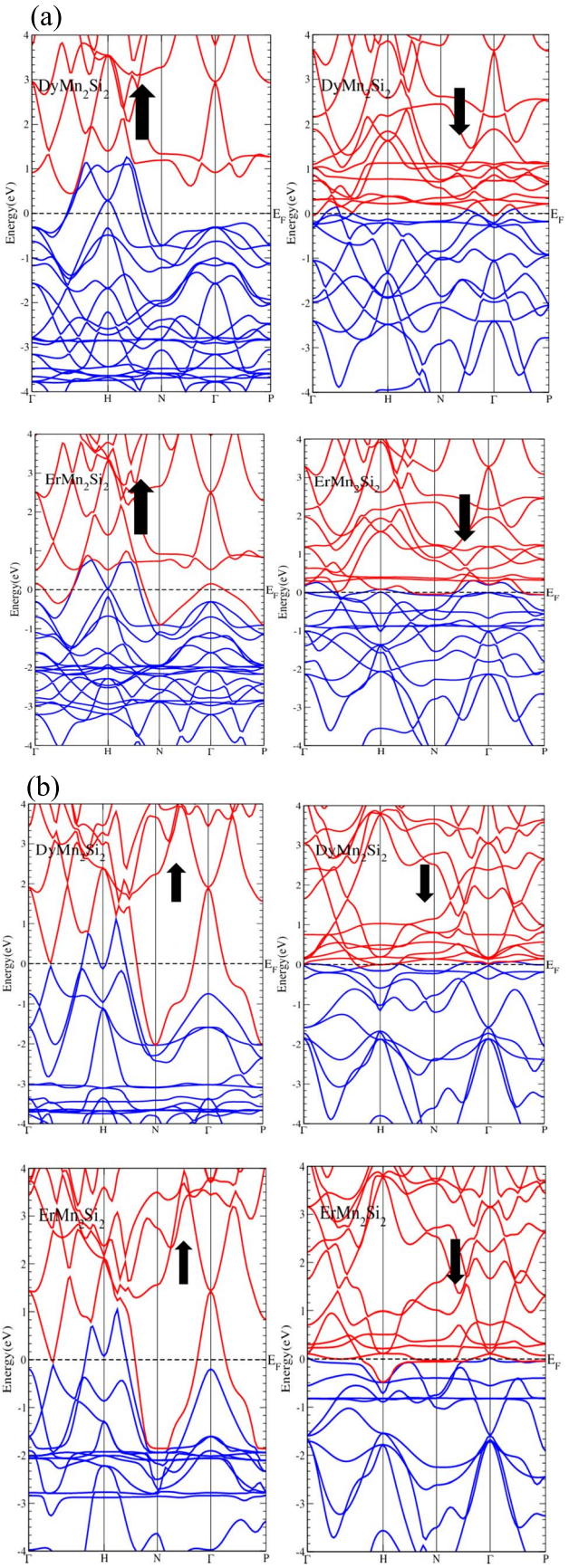

Figure 3. (a) Band structure of XMn_2Si_2 (X=Dy, Er) Compounds in ferromagnetic phase by using PBE-GGA approximations. (b) Band structure of $DyMn_2Si_2$ and $ErMn_2Si_2$ Compound in ferromagnetic phase by GGA+U approximations.

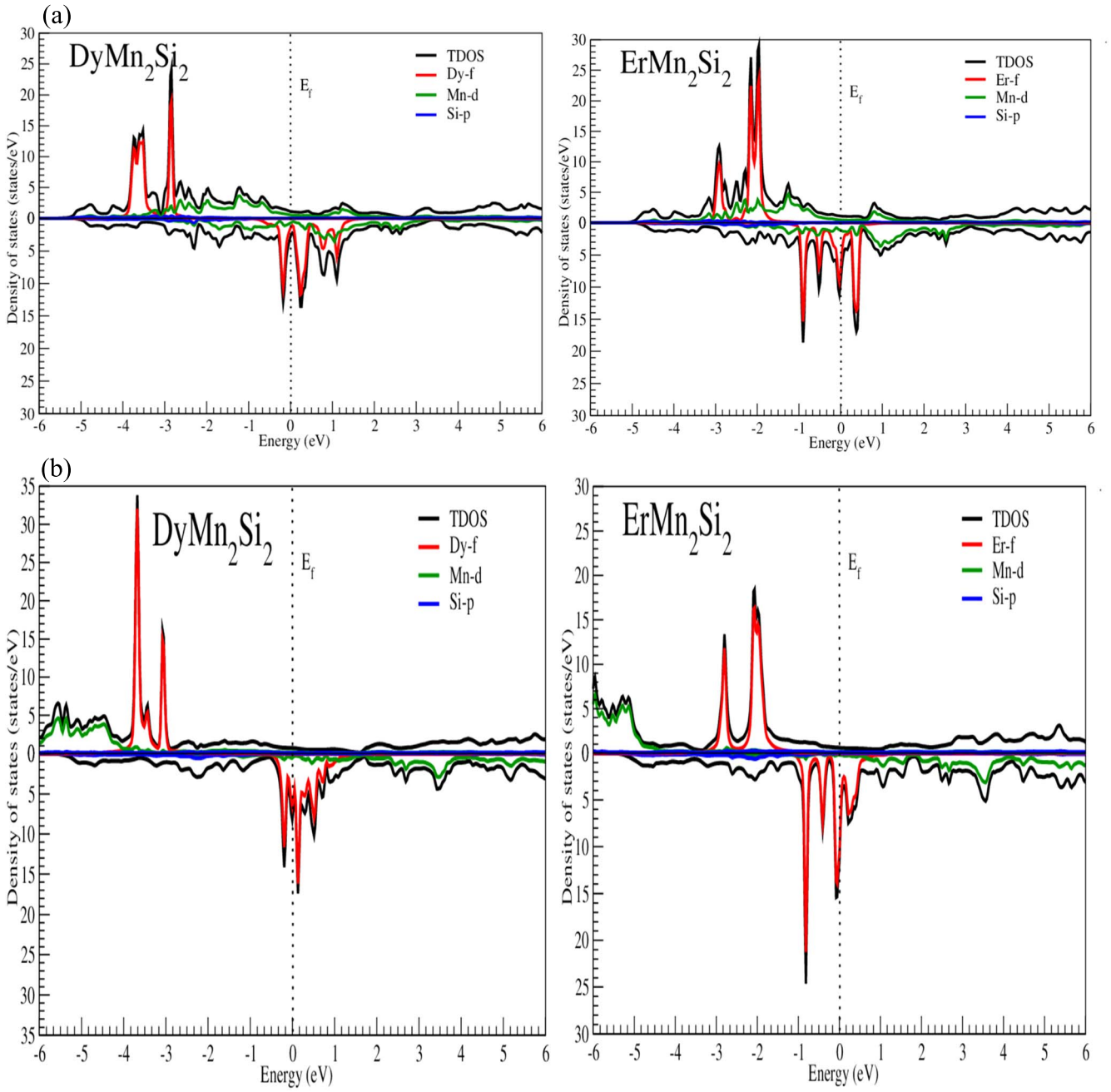

Figure 4. (a) Density of State (DOS) XMn_2Si_2 (X=Dy, Er) Compounds in ferromagnetic phase by using PBE-GGA approximations. (b) Density of State (DOS) XMn_2Si_2 (X=Dy, Er) Compounds in ferromagnetic phase by GGA+U approximations.

temperatures, the $ErMn_2Si_2$ compound exhibited the highest value of electrical conductivity when compared to $DyMn_2Si_2$. Even in high-temperature zones, rare-Earth-based materials XMn_2Si_2 show no growth in the value of the electrical conductivity curve as the temperature rises.

Less heat conductivity is necessary for excellent thermoelectric materials. Figure 6 shows that the thermal conductivity curves for the rare-Earth based material XMn_2Si_2 are increasing across the full temperature range (300–800 K). When contrasted to the plot of electrical conductivity to opposing fluctuation patterns in the thermal conductivity[62] of certain compounds, the Wiedemann–Franz law cannot be proven. The thermal conductivity curves began with a similar lower value for both the compounds at a temperature of around 50 K and progressively climbed with temperature while sharing the same magnitudes in the range of 250–350 K until reaching their highest value at a temperature of about 800 K.

In addition, XMn_2Si_2 where (X=Dy, Er) compounds showed minimum and maximum values of thermal conductivity at high temperatures (800 K). Consequently, materials with poor heat conductivity can be crucial for a variety of applications.[4,50,62] The electrical conductivity in Fig. 5 basically follows the exact opposite trend.

We may learn more about the nature or kind of material by using the Seebeck coefficient. Figure 7 shows that the Seebeck coefficient curves of XMn_2Si_2 (X=Dy, Er) initially started with the maximum values and tend to decrease gradually, where a clear upward and downward hump appear in the S curve (negative region) over the mentioned temperature range of 0 to 800 K. The Past few studies calculated the transport properties in the same manner as we investigated in this work. Further they have reported positive/negative Seebeck coefficient with high ZT as well for the same and different class of the compounds.[4,14,16,63,64]

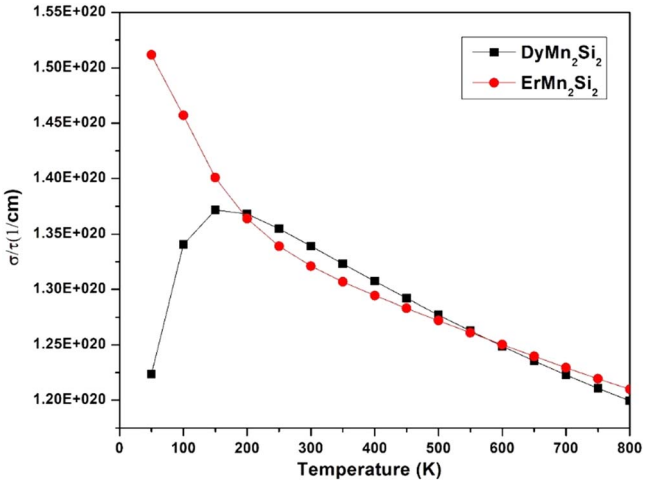

Figure 5. Variation of Electrical Conductivity with respect to temperature for XMn_2Si_2 (X=Dy, Er) Compounds.

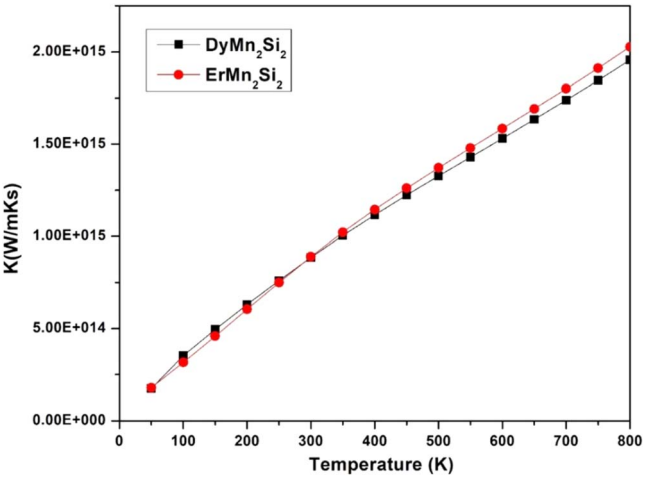

Figure 6. Variation of thermal-Conductivity for XMn_2Si_2 (X=Dy, Er) Compounds with respect to temperature.

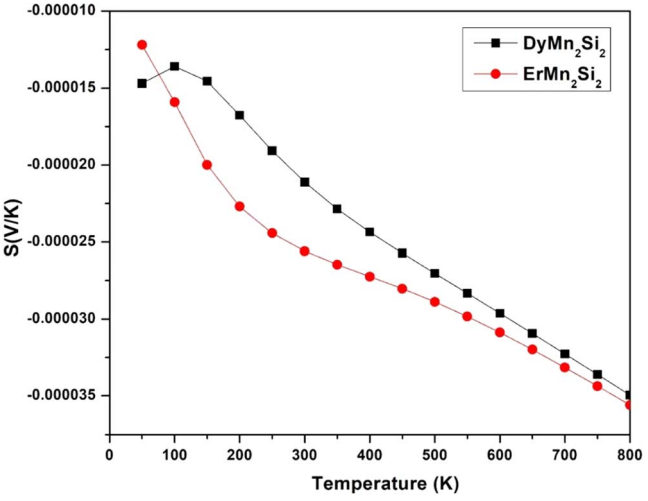

Figure 7. Variation of Seebeck coefficient (S) with respect to temperature for XMn_2Si_2 (X=Dy, Er) Compounds.

These compounds display negative values for the Seebeck coefficient (S) over the whole range of temperature, XMn_2Si_2 exhibits n-type conduction performance because of negative sign

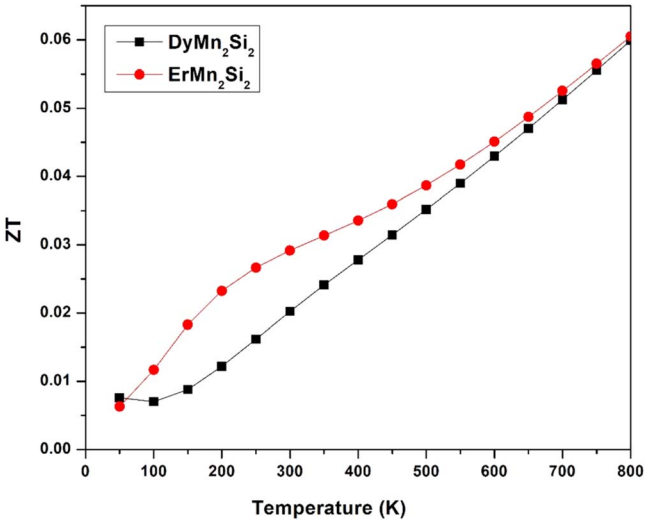

Figure 8. Variation of ZT with respect to temperature for XMn_2Si_2 (X=Dy, Er) Compounds.

appeared at the moment of observation here on plotted data. These electron carriers predominate in electronic transport. Additionally, across the indicated temperature range, the $DyMn_2Si_2$ compound has the highest value of the Seebeck coefficient of the two understudied compounds.

By using the figure of merit (ZT), the thermoelectric performance was estimated. A material with a high ZT value is more effective. As seen in Fig. 8, the rare-Earth based XMn_2Si_2 compound's ZT curves begin at their minimum values, which is thought to be the lower values at around 50 K. When a temperature is raised further, the ZT curves for $DyMn_2Si_2$/$ErMn_2Si_2$ are gradually/dramatically increased till 400 K. Further onward, in the high temperature range, both the spectra increase linearly with temperature and reach their maximum value at 800 K. The similar behaviour of ZT with Seebeck coefficient were observed in few other studies for the same and different class of the materials.[4,14,16,63,64]

Furthermore, Er-based compounds have a high ZT value in magnitude at 800 K, which means the material response in a high temperature range is significant as compared to $DyMn_2Si_2$. The $ErMn_2Si_2$ is a viable contender for high-temperature applications in waste heat management because of its high ZT values in the high-temperature region in thermoelectric devices.

Conclusions

In this research work, DFT calculations are performed by using different approximations (PBE-GGA and GGA+U) to study the structural, thermoelectric, electronic, and magnetic properties of pristine rare-Earth based $DyMn_2Si_2$, and $ErMn_2Si_2$ compounds. The calculated parameters like lattice constants and the stable structure optimization in the FM phase are reliable with other experimental reported results. The designed band structures organized by DOS plots announce complete metallic-character by robust hybridization appearances between Dy/Er-f and Mn-d states in the valence band and the Si-p state in the conduction band. Similarly, the attained entire magnetic-moments align parallel to the over-all ferromagnetic direction (by both potentials), which reveals stronger ferro-magnetism in the examined pristine intermetallic Rare-Earth based compounds. Furthermore, Er-based compounds have high ZT and high electrical and thermal conductivities values in magnitude at 800 K, which means the $ErMn_2Si_2$ material response in a high temperature range in thermo-electric devices is significant as compared to $DyMn_2Si_2$.

ORCID

Ali H. Reshak https://orcid.org/0000-0001-9426-8363

References

1. L. M. Schetky, *MRS Bull.*, **21**, 50 (1996).
2. A. A. Khan et al., *Chin. J. Phys.*, **77**, 956 (2022).
3. Z. Zada et al., *Indian J. Phys.*, **96**, 3151 (2022).
4. A. A. Khan et al., *The European Physical Journal Plus*, **137**, 351 (2022).
5. Z. Zada et al., *J. Mol. Struct.*, **1252**, 132136 (2022).
6. V. Sechovský, L. Havela, K. Prokeš, H. Nakotte, F. R. De Boer, and E. Brück, *J. Appl. Phys.*, **76**, 6913 (1994).
7. Z. Zada, R. Zada, A. A. Khan, M. Saqib, M. F. U. Rehman, M. Ismail, N. Kulhari, K. S. Sharma, X. Shen, and M. Faizan, *J. Mol. Struct.*, **1268**, 133698 (2022).
8. R. Bibi et al., *J. Solid State Chem.*, **302**, 122388 (2021).
9. Z. Zada, A. Laref, G. Murtaza, A. Zeb, and A. Yar, *Int. J. Mod. Phys. B*, **33**, 1950199 (2019).
10. Z. Zada, H. Ullah, R. Bibi, S. Zada, and A. Mahmood, *Z. Naturforsch. A*, **75**, 543 (2020).
11. M. Siddique, A. Iqbal, A. U. Rahman, S. Azam, Z. Zada, and N. Talat, *Nuclear Engineering and Technology*, **53**, 592 (2021).
12. Z. Zada et al., *The European Physical Journal Plus*, **136**, 1 (2021).
13. A. A. Khan, W. Khan, A. Khan, A. Laref, A. Zeb, and G. Murtaza, *Mater. Res. Express*, **6**, 066102 (2019).
14. Z. Zada et al., *Physica B*, **607**, 412866 (2021).
15. A. Hirohata and K. Takanashi, *J. Phys. D: Appl. Phys.*, **47**, 193001 (2014).
16. A. A. Khan et al., *Phys. Scr.*, **97**, 065810 (2022).
17. J. A. Brug, T. C. Anthony, and J. H. Nickel, *MRS Bull.*, **21**, 23 (1996).
18. N. P. Kolmakova, A. A. Sidorenko, and R. Z. Levitin, *Low Temp. Phys.*, **28**, 653 (2002).
19. L. Li, B. Saensunon, W. D. Hutchison, D. Huo, and K. Nishimura, *J. Alloys Compd.*, **582**, 670 (2014).
20. L. Li, K. Nishimura, W. D. Hutchison, Z. Qian, D. Huo, and T. NamiKi, *Appl. Phys. Lett.*, **100**, 152403 (2012).
21. J. L. Wang et al., *J. Phys. Condens. Matter*, **25**, 386003 (2013).
22. G. Li, J. Wang, Z. Cheng, Q. Ren, C. Fang, and S. Dou, *Appl. Phys. Lett.*, **106**, 182405 (2015).
23. Z. J. Mo, *J. Appl. Phys.*, **115**, 073905 (2014).
24. D. Rossi, R. Marazza, D. Mazzone, and R. Ferro, *J. Less-Common Met.*, **59**, 79 (1978).
25. A. Szytuła and I. Szott, *Solid State Commun.*, **40**, 199 (1981).
26. H. Onodera, M. Ohashi, H. Yamauchi, Y. Yamaguchi, and H. Kobayashi, *J. Magn. Magn. Mater.*, **109**, 249 (1992).
27. T. Ono et al., *J. Magn. Magn. Mater.*, **123**, 133 (1993).
28. K. Kudou, *J. Alloys Compd.*, **358**, 182 (2003).
29. D. C. Dos Reis, *J. Magn. Magn. Mater.*, **424**, 84 (2017).
30. K. A. Gschneidner Jr and L. Eyring, *Handbook on the Physics & Chemistry of Rase Earths* (North-Holland, Amsterdam) 6, 212 (1984).
31. D. Rossi, R. Marazza, and R. Ferro, *J. Less-Common Met.*, **58**, 203 (1978).
32. S. Okada et al., *J. Alloys Compd.*, **383**, 254 (2004).
33. S. Okada et al., *Jpn. J. Appl. Phys.*, **41**, 555 (2002).
34. W. Bażela, *J. Alloys Compd.*, **442**, 132 (2007).
35. D. C. Dos Reis et al., *J. Supercond. Novel Magn.*, **33**, 3773 (2020).
36. H. Kobayashi, H. Onodera, and H. Yamamoto, *J. Magn. Magn. Mater.*, **109**, 17 (1992).
37. M. Ohashi, H. Onodera, T. Ono, T. Andow, S. Funahashi, Y. Yamaguchi, and H. Kobayashi, *Proceedings of the Fifth International Symposium on Advanced Nuclear Energy Research Neutrons as Microscopic Probes*(Tokyo, Japan)**404** (1993).
38. K. S. V. L. Narasimhan, V. U. S. Rao, R. L. Bergner, and W. E. Wallace, *J. Appl. Phys.*, **46**, 4957 (1975).
39. S. G. Sankar, S. K. Malik, V. U. S. Rao, and R. Obermyer, *AIP Conference Proceedings*, **34**, 236 (1976).
40. A. M. Umarji, D. R. Noakes, P. J. Viccaro, G. K. Shenoy, A. T. Aldred, and D. Niarchos, *J. Magn. Magn. Mater.*, **36**, 61 (1983).
41. J. Leciejewicz, S. Siek, and A. SzytułLa, *J. Magn. Magn. Mater.*, **40**, 265 (1984).
42. M. S. Kim, N. H. Sung, Y. Son, M. S. Ko, and B. K. Cho, *Appl. Phys. Lett.*, **98**, 172509 (2011).
43. L. Li, K. Nishimura, and H. Yamane, *Appl. Phys. Lett.*, **94**, 102509 (2009).
44. J. L. Wang, S. J. Campbell, J. M. Cadogan, A. J. Studer, R. Zeng, and S. X. Dou, *Appl. Phys. Lett.*, **98**, 232509 (2011).
45. T. Fujiwara, H. Fujii, and T. Shigeoka, *Physical Review B*, **63**, 174440 (2001).
46. A. A. Khan, R. Hasil, A. Laref, N. Ullah, M. Sajjad, A. Zeb, and G. Murtaza, *Solid State Commun.*, **300**, 113667 (2019).
47. G. Murtaza, A. A. Khan, M. Yaseen, A. Laref, N. Ullah, and I. ur Rahman, *Chin. Phys. B*, **27**, 047102 (2018).
48. Z. Khan, G. Murtaza, A. A. Khan, A. Laref, N. A. Kattan, and M. Haneef, *Int. J. Energy Res.*, **45**, 7703 (2021).
49. I. Rahim et al., *Digest Journal of Nanomaterials & Biostructures (DJNB)*, **16** (2021).
50. G. Murtaza, A. A. Khan, M. M. AL-Anazy, A. Laref, Q. Mahmood, Z. Zada, and M. Aman, *The European Physical Journal Plus*, **136**, 1 (2021).
51. P. Blaha, K. Schwarz, G. K. Madsen, D. Kvasnicka, and J. Luitz, *wien2k, An augmented plane wave+ local orbitals program for calculating crystal properties* (2001).
52. J. P. Perdew, K. Burke, and M. Ernzerhof, *Phys. Rev. Lett.*, **77**, 3865 (1996).
53. A. I. Liechtenstein, V. I. Anisimov, and J. Zaanen, *Physical Review B*, **52**, R5467 (1995).
54. O. Bengone, M. Alouani, P. Blöchl, and J. Hugel, *Physical Review B*, **62**, 16392 (2000).
55. A. A. Khan, M. Yaseen, A. Laref, and G. Murtaza, *Physica B*, **541**, 24 (2018).
56. H. J. Monkhorst and J. D. Pack, *Physical review B*, **13**, 5188 (1976).
57. A. A. Khan, A. U. Rehman, A. Laref, M. Yousaf, and G. Murtaza, *Z. Naturforsch. A*, **73**, 965 (2018).
58. J. D. Pack and H. J. Monkhorst, *Physical Review B*, **16**, 1748 (1977).
59. G. K. Madsen, *JACS*, **128**, 12140 (2006).
60. A. A. Khan et al., *Int. J. Energy Res.*, **45**, 13657 (2021).
61. K. S. V. L. Narasimhan, V. U. S. Rao, W. E. Wallace, and I. Pop, *AIP Conf. Proc.* 29, 594(American Institute of Physics) (1976).
62. X. Du, L. Mihaly, and P. B. Allen, *Physica B*, **194**, 1507 (1994).
63. Z. Zada et al., *Physica B*, **649**, 414470 (2023).
64. A. A. Khan et al., *Mater. Chem. Phys.*, 127422 (2023).